Sheffield Hallam University

Hybrid HIPIMS and DC magnetron sputtering deposition of TiN coatings: Deposition rate, structure and tribological properties

LUO, Quanshun <http://orcid.org/0000-0003-4102-2129>, YANG, S. and COOKE, K.E.

Citation:

Hybrid HIPIMS and DC magnetron sputtering deposition of TiN coatings: deposition rate, structure and tribological properties

Q. Luo[1], S. Yang[2], K. E. Cooke[2]

[1]*Materials and Engineering Research Institute, Sheffield Hallam University, Howard Street, Sheffield, S1 1WB, UK*

[2]*Teer Coatings Ltd., Miba Coating Group, West Stone House, West Stone, Berry Hill Industrial Estate, Droitwich, Worcestershire WR9 9AS, UK*

Abstract:
High power impulse magnetron sputtering (HIPIMS) has the advantage of ultra-dense plasma deposition environment although the resultant deposition rate is significantly low. By using a closed field unbalanced magnetron sputtering system, a hybrid process consisting of one HIPIMS powered magnetron and three DC magnetrons has been introduced in the reactive sputtering deposition of a TiN hard coating on a hardened steel substrate, to investigate the effect of HIPIMS incorporation on the deposition rate and on the microstructure and mechanical and tribological properties of the deposited coating. Various characterizations and tests have been applied in the study, including XRD, FEG-SEM, cross-sectional TEM, Knoop hardness, adhesion tests and un-lubricated ball-on-disk tribo-tests. The results revealed that, both the DC magnetron and hybrid-sputtered TiN coatings exhibited dense columnar morphology, a single NaCl-type cubic crystalline phase with strong (220) texture, and good adhesion property. The two coatings showed similar dry sliding friction coefficient of 0.8 – 0.9 and comparable wear coefficient in the range of $1 - 2 \times 10^{-15}$ $m^3N^{-1}m^{-1}$. The overall deposition rate of the hybrid sputtering, being 0.047 µm/min as measured in this study, was governed predominantly by the three DC magnetrons whereas the HIPIMS only made a marginal contribution. However, the incorporated HIPIMS has been found to lead to remarkable reduction of the compressive residual stress from -6.0 to -3.5 GPa and a slight increase in the coating hardness from 34.8 to 38.0 GPa.
Key Words: Magnetron sputtering deposition; HIPIMS; TiN; TEM; Friction and wear

1 Introduction

High power impulse magnetron sputtering (HIPIMS), also called HPPMS (high power pulsed magnetron sputtering), has been known for its capability of achieving extremely dense plasma with high ionization ratio, and high pulsed peak ion current densities. For example, by using a pulsed power supply at a peak power density of 2,800 $W \cdot cm^{-2}$ with a copper target, an extremely intense plasma with peak ion current densities of 3.4 $A \cdot cm^{-2}$ was achieved along with a reported ionization ratio of the deposited Cu flux as high as 70% [1]. In fact, initial studies on pulsed magnetrons dated back from 1970s till later 1990s when it was demonstrated that, operating a conventional magnetron sputtering source in a pulsed mode could lead to a pulsed target current having a peak magnitude two orders higher than the average current in a conventional sputtering mode [2-8]. Since early 1990s, sputtering techniques based on pulsed DC glow discharge have been developed for the deposition of thin films [1, 8-9]. Up to now, HIPIMS technology has been widely recognized in coating deposition on complex-shape substrates, the enhancement of interface adhesion, and improved structure control of dense coatings [10-12].

However, early HIPIMS technology was associated with substantially lower deposition rates than other magnetron sputtering techniques [13-15]. Comparative experimental studies have been carried out to compare the deposition rates of HIPIMS or HPPMS deposition and the direct current (DC) magnetron sputtering of the same average target current [13-14]. It was found that, the HPPMS deposition rates were equal to DC magnetron before reaching a peak target current density, e.g. at about 570 $mA \cdot cm^{-2}$, followed by a pronounced decrease in the deposition rates accompanying further increase of the

current density [13]. Experimental and numerical modelling investigations suggested that, the causes of the lower deposition rates of HIPIMS process were found to result from both the back-attraction of ionized species as well as gas depletion of the process gas during the HIPIMS pulse [15]. Obviously, the low deposition rate has been a major barrier for the commercial applications of HIPIMS.

Recently efforts have been made to increase the deposition rates of the HIPIMS process by either adjusting the HIPIMS power input to moderate levels [16-17], developing a hybrid deposition process [18-20], or varying the magnetic field [16, 21-22]. In the first approach [16-17], the main differences between the HIPIMS (or HPPMS) and the modulated pulse power (MPP) technique include the magnitude, duration, and shape of the high power pulse. The density of the pulse power was moderated typically to 0.5 – 1.5 $kW \cdot cm^{-2}$ as compared to 1.0 – 3.0 $kW \cdot cm^{-2}$ in the HPPMS process, whereas the pulse length was significantly prolonged up to 3,000 µs as compared to 100 – 150 µs in the HPPMS process. The MPP technique provides a controlled low ion energy and high metal-ion flux for the deposition of dense coatings with good adhesion property. Moreover, this technique has also demonstrated its potential in the deposition of thick metal nitride coatings with dense nano-columnar structure and controlled low compressive residual stresses [17]. In the second approach, a HIPIMS power supply has been introduced to a multi-target deposition system to combine with another deposition technique having higher deposition rates, e.g. DC magnetron sputtering. In the hybrid deposition, a reasonably high overall deposition rate can be achieved because of the predominant role of the DC magnetrons in the deposition rate [18]. Meanwhile, it has been reported that the incorporated HIPIMS component brought about

changes in the texture, hardness and residual stress of the coatings [18]. An example of HIPIMS induced structural changes has been recently reported in the deposition of high-AlN-content meta-stable TiAlN coatings by using a hybrid process of HIPIMS and DC magnetron, in which remarkably different Ti-Al-N coatings have been grown when the HIPIMS was applied to the Al or Ti target [19]. When the HIPIMS was applied to the Al target, the deposited coating exhibited single-phase $Ti_{1-x}Al_xN$ (x = 0.55 – 0.60) cubic crystalline structure, high hardness of up to 30 GPa, and a low tensile residual stress of 0.2 – 0.7 GPa. When the HIPIMS was applied to the Ti target, however, the deposited coating showed a two-phase crystalline structure of cubic TiAlN and hexagonal AlN which exhibited lower hardness of only 18 – 19 GPa and substantially higher compressive stress up to 2.7 GPa. Finally, the magnetic field strength has significant influence on the deposition rate of the modulated pulsed power magnetron sputtering [21-22]. Higher ratio of the actual deposition rates of the pulsed power magnetron sputtering to DC magnetron sputtering has been obtained at reduced magnetic field strength, which is strongly material dependent for a range of target materials of copper, aluminium, chromium, titanium and tantalum [21]. However, the increased deposition rate is accompanied with the decrease in the ionization of metal and gas species which consequently affects the microstructure and mechanical properties of the deposited films. In literature [22], preliminary results were reported on magnetron sputtering of a Al target in HIPIMS mode using a low A low strength radio frequency (RF) magnetic array. The magnetic field design of the RF magnetic array showed a deposition rate substantially the same as that obtained for the 'standard' strength balanced array and DC power as a result of the increased sputtered flux transport perpendicular to the target surface.

Recently, we have developed a multi-target hybrid deposition technique, using HIPIMS and close field unbalanced magnetron sputtering (CFUBMS) deposition, in the fabrication of TiMoN multilayer coatings [20]. In this paper, a comparative study is reported on TiN coatings grown by the hybrid process and by pure DC magnetron sputtering respectively, to investigate the effect of HIPIMS on the structure and properties of the deposited coating. Cross-sectional transmission electron microscopy (XTEM), X-ray diffraction (XRD) and field emission gun scanning electron microscopy (FEG-SEM) were employed in the coating characterization, while the mechanical and tribological properties of the coatings were evaluated by Knoop indentation and un-lubricated ball-on-disk tribo-tests respectively. It has been found that, in addition to the obtained reasonably high deposition rate, the incorporated HIPIMS power supply resulted in some favourable changes in the structure and properties of the deposited coatings.

2 Experimental
2.1 Deposition

Flat samples of hardened M42 tool steel (64 HRC) and AISI 316L stainless steel were coated using a CFUBMS coating system. Figure 1 shows a schematic diagram of the 4-magnetron system, in which pure titanium targets
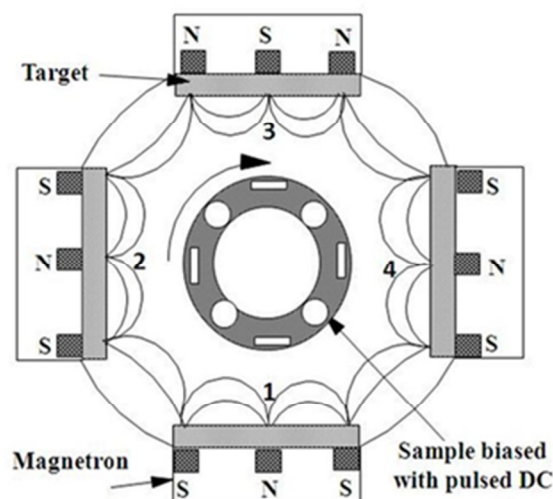

Fig. 1 Schematic diagram of the four Ti targets closed field unbalanced magnetron sputtering ion plating system: one target is connected to a HIPIMS power supply and the other three operated in a conventional DC-Magnetron mode.

(dimensions of 100 mm in width and 300 mm in height) were used in combination with a partial pressure of gaseous nitrogen to grow the TiN hard coatings reactively. One type of TiN was deposited using standard DC power supplies on all the four magnetrons (referred to here as '4DC'). The second type was produced by using such a magnetron configuration that one of the four magnetrons was supplied with a HIPIMS power unit (HMP 1/1 model) and the other three were supplied by the existing DC power supplies (referred to here as "3DC+1HIPIMS"). During the whole deposition process, the sample stage rotated at a fixed speed of 4 rpm.

The deposition procedures started with ion etching on the samples using pulsed DC power applied to the substrates on their turntable with parameters of: frequency 350.0 kHz, pulse width 0.5 µs, and a high negative potential of -400 V. For the case of 4DC magnetrons, the ion etching was dominated by argon ions (Ar^+) without net deposition of Ti, when all magnetrons were powered at a low level of 0.1 kW. For the case of the 3DC+1HIPIMS, the HIPIMS generator connected to one of the Ti targets has a maximum capacity of voltage 1,000 V, peak current 1,000 A and total mean power 100,000 W. In this case, it was operated at the HMP 1/1 model at the output power parameters of mean current 4 A, mean voltage 750 V and mean power 3.0 kW (an equivalent power density of 50 W·cm^{-2} on the plasma track at the target). The pulse current wave forms were 2×225 Hz frequency and pulse width of 100 µs. The target size was 100×300 mm whereas the measured track area was 200×15 mm. The other three DC magnetrons were remained at the low power level of 0.1 kW. Therefore both argon ions and a high ratio of metallic ions (Ti+/Ti neutral) could be produced, as described by Kouznetsov [1].

Following the ion etching, the second stage was to deposit the coating: a metallic titanium adhesion layer followed by a titanium nitride layer. In the deposition, all the four magnetrons were powered at 3.0 kW for both the 4DC and the 3DC+1HIPIMS experiments. Meanwhile, the negative bias potential of the substrate was reduced to -70 V to start

the net deposition of Ti coating. The HIPIMS parameters were same as those applied in the etching stage. After that, reactive nitrogen gas was then introduced in the deposition to produce first a graded interlayer and then to deposit monolithic constant stoichiometric TiN hard coatings in both the cases of 4DC and 3DC+1HIPIMS, until the deposition process was terminated. The deposition times for the TiN deposition were 40 and 55 minutes for the 4DC and 3DC+1HIPIMS respectively, to obtain TiN coatings with similar thickness.

2.2 Characterization

The TiN coatings deposited on the stainless steel substrate were characterized using SEM, XRD and XTEM. A FEI Nova200 FEG-SEM was employed to observe both the as-deposited coating surfaces and the cross-sections. Coating thickness was determined from the cross-sectional images. The instrument was operated at 15 kV and spot 3. A computer programmed Philips X'Pert X-ray diffraction instrument was used to characterize the crystallographic properties and to determine the residual stress, using the X-ray Cu-K$_{\alpha 1}$ (λ= 0.154056 nm) with the copper anode being powered at 40 kV and 40 mA. In the crystallographic characterization, the instrument was run at the Bragg-Brentano (θ-2θ) mode at a step size 0.03^0 and step scanning time 300 seconds for the period of 2θ = 30^0 - 120^0. In the measurement of residual stress, the sin$^2\psi$ technique was employed based on slow scans of the (111) and (220) planes at step size of 0.033^0 and step time of 300 - 700 seconds respectively. The diffraction peak positions were determined by the parabolic approach following our recent optimization of XRD residual stress measurement [23]. The Young's modulus and Poisson's ratio values were taken from literature to be 300 GPa and 0.23 respectively [23]. A Philips CM20 TEM was used to characterize the cross-sectional structure of the deposited coatings. The instrument has a W-filament and was operated at 200 kV. The cross-sectional samples were prepared by low angle Ar-ion milling using a Gatan 691 precision ion polishing system. More details of the sample preparation techniques can be found in the authors' previous publication [24].

2.3 Mechanical and tribological evaluations

The mechanical and tribological evaluations were carried out on the TiN coatings deposited on the hardened M42 tool steel substrate. A Mitituyo HV/HK micro-hardness tester was employed to measure the Knoop hardness at an indentation load of 25 g. Ten indents were measured on each sample to obtained an average value and the associated standard deviation. A Rockwell hardness tester and a Teer ST3100 scratch tester were employed to evaluate the adhesion property. For the Rockwell indentation, an applied load of 150 kg was used. The scratch adhesion test was conducted using a 200 µm radius conical Rockwell diamond at a normal load increasing linearly with the scratching distance, up to a maximum of 60 N, when the test was terminated to avoid damage to the diamond. Subsequently the resulting indentations and scratches were examined using an optical microscope to evaluate the adhesive delamination behaviour, qualitatively and quantitatively.

The friction and wear properties were tested using a Teer POD-1 pin-on-disc tribometer. The testing conditions included a 5.0 mm diameter WC-8% Co ball as the sliding counterpart, applied normal load of 5 N, a constant linear sliding speed of 100 mm/s for three sliding wear tracks on the coated disk having nominal diameters of 6 and 10 mm, respectively, under room temperature conditions and with a relative humidity in the range RH 30-40%. For each tribotest the sliding time was 70 minutes. The resulting wear tracks were sectioned and measured using a ball-crater taper section technique to quantify the wear depth and hence to allow the calculation of wear volume loss.

3 Results

3.1 Mechanical properties

The TiN coatings grown by the 4DC and 3DC+1HIPIMS processes showed Knoop hardness of 34.8 ± 3.8 GPa and 38.0 ± 5.2 GPa respectively. The 3DC+1HIPIMS grown TiN is slightly harder than the DC magnetron TiN, whereas the small increment of 3.2 GPa is comparable to the measurement derivation. In both the Rockwell indentation and the scratch tests, both coatings exhibited good adhesion property. The resulting indents and scratches are shown in Figure 2. Both coatings exhibited no adhesive failure, which was true even at the scratching ends corresponding to the maximum scratch load of 60 N. The applied indenting and scratching loads only resulted in coating cracks following plastic deformation of the relatively softer substrates.

3.2 Structure characterization

Figure 3 shows ion-beam-polished cross-sections of the TiN coatings. The metallic Ti base layer in both cases was approximately 230 nm in thickness. This value was estimated first from the SEM image contrast and then confirmed by XTEM observation (to be shown later). The
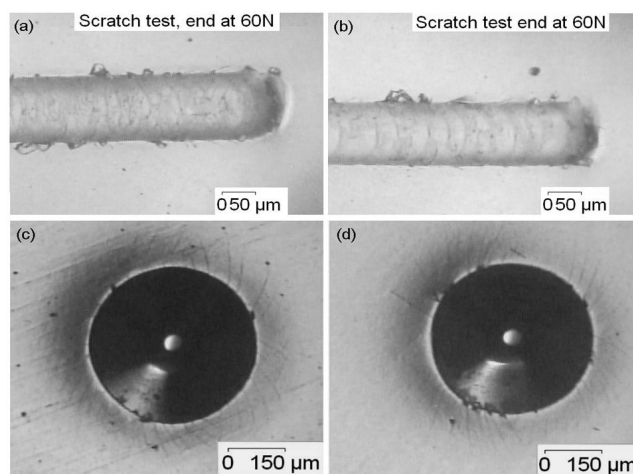

Fig. 2 Optical micrographs showing the adhesion of the TiN coatings: (a) the TiN grown by 4DC magnetrons; and (b) the TiN grown by 3DC + 1HIPIMS.
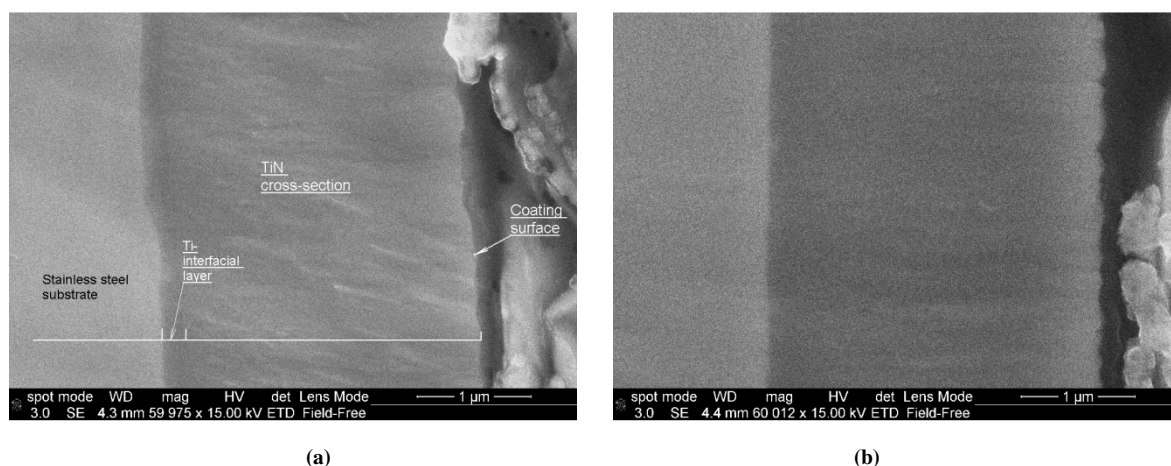
(a) **(b)**

Fig. 3 SEM images of the ion-beam polished cross-section: (a) the TiN grown by 4DC magnetrons; and (b) the TiN grown by 3DC + 1HIPIMS.
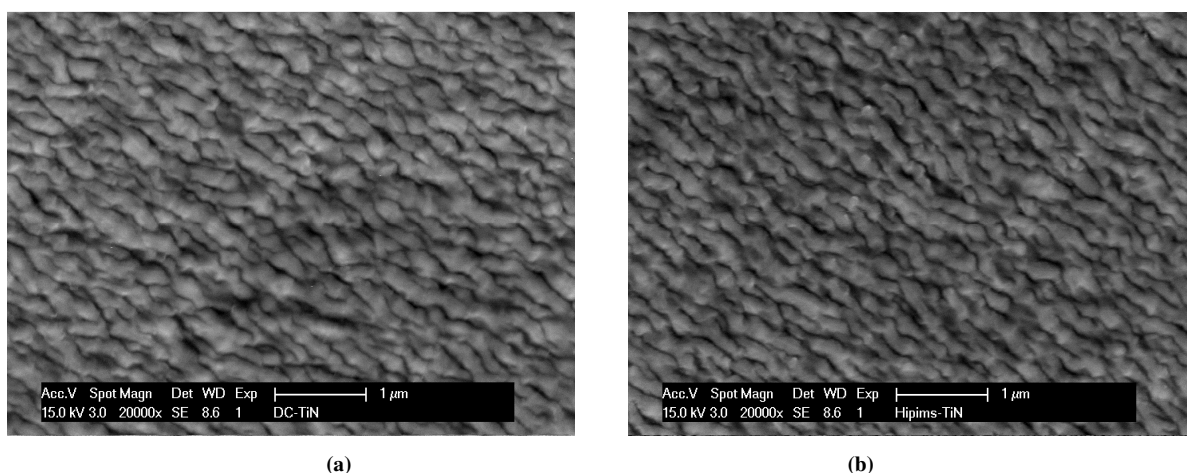

(a) **(b)**

Fig. 4 SEM images of the coating surfaces: (a) TiN grown by 4DC magnetrons; and (b) TiN grown by 3DC+HIPIMS. Note the similar wave-like roughness features.
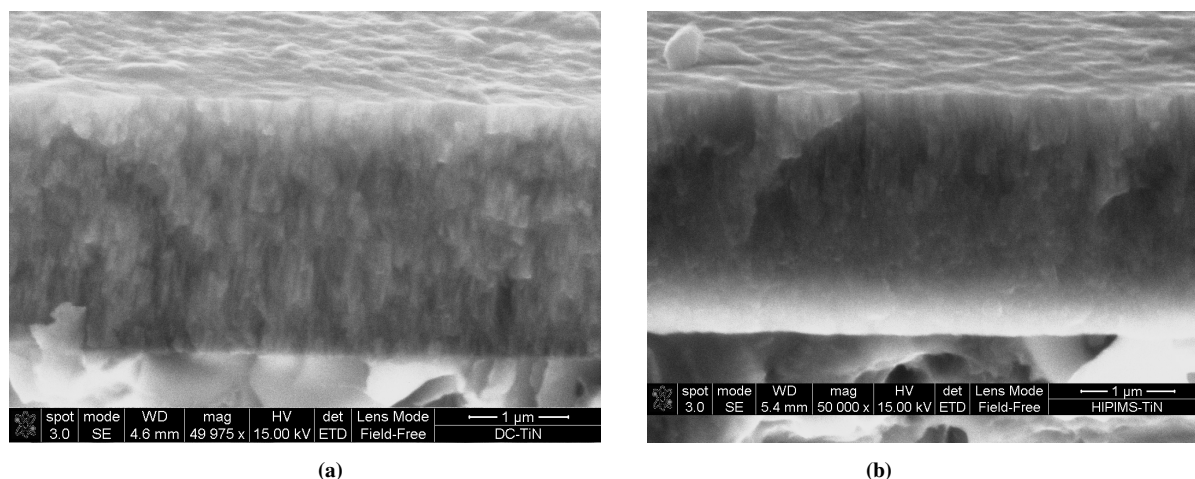

(a) **(b)**

Fig. 5 SEM images of the fractured cross-sections: (a) TiN grown by 4DC magnetrons; and (b) TiN grown by 3DC+HIPIMS. Note the extremely fine columnar grains across the coating sections, especially the modified morphology in the middle thickness range of the latter.

corresponding thickness of the TiN top-coats was measured to be 2.56 µm and 2.69 µm for the 4DC and 3DC+1HIPIMS coatings respectively. In the 4DC magnetron coating, the deposition rate can be determined to be 0.064 µm/min, or 0.016 µm/min per magnetron (each powered at 3kW). In contrast, the 3DC+1HIPIMS

deposition achieved an overall deposition rate of 0.049 µm/min.

Figure 4 shows SEM micrographs of the coating surfaces. Both coatings exhibit similar nano scale waviness, almost identical to each other. The wave-like patterns correspond to the rough fronts of columnar growth as a

result of relatively moderate ion bombardment conditions. Similar phenomena were found in other coatings grown by magnetron sputtering under similar conditions of low atomic mobility [24-27]. Such columnar morphology has been observed on fractured cross-sections, Figure 5. In Figure 5a, the coating grown by 4DC magnetron sputtering shows extremely fine and short columns. Typical widths of the short columnar grains are less than 100 nm. Such structure features indicates a mode of interrupted columnar growth, indicative of re-nucleation during the coating growth. In Figure 5b, the coating grown by 3DC+HIPIMS also shows nano-scale short columns across the fractured section, whereas the grain sizes are even smaller. Especially, the grain sizes in the middle-thickness range were too small to be resolved by the FEG-SEM. The different columnar grain sizes suggest that, the incorporated HIPIMS led to grain refining during the coating growth.

Figures 6 shows XTEM observation and selected area diffraction (SAD) analysis of the 4DC magnetron sputtered TiN coating. In Figure 6a, the coating shows a layered structure, following the sequence of deposition, from an ion-mixing interfacial layer, the Ti interlayer, and the TiN coating. The interfacial ion-mixing layer between the substrate and the Ti interlayer can be revealed in the bright-field TEM imaging to be approximately 30 ~ 50 nm thick, void-free, and incoherent to both the adjacent substrate and Ti-layer. The interfacial film is likely to give rise to strong adhesion of the deposited coating to the substrate because of the intermixing between the incident Ti/Ar ions with the substrate surface layer. Such interfacial strengthening is

well known in cathodic arc etching. For example, previous research has revealed that Cr-ion etching of a steel substrate surface under cathodic glow discharge mode caused ion implantation in the top substrate surface or an intermixed Cr-Fe layer [28-29]. Following the interfacial layer, the Ti interlayer is approximately 200 – 250 nm thick, exhibiting well-defined polycrystalline columnar or equaxial granular morphology. Then upon the Ti interlayer, the initial TiN coating exhibits cross-sectional morphology of short columnar grains. The columnar grains, however, show less-defined grain boundaries. This could be attributed to the high density of lattice distortion caused by the entrapped nitrogen in the TiN coating. In the upper part, Figure 6b, the TiN coating still exhibits columnar morphology whereas the remarkably coarser columns have well-defined grain boundaries. In addition, the whole section of the coating showed absolutely void-free density in the TEM observation in exception of an inter-column crack obviously caused by the sample preparation (seeing Figure 6a). Figure 6c is a SAD pattern of the TiN coating. It indicates predominantly a NaCl-type cubic crystalline structure with well-defined diffraction rings of {111}, {200}, and {220} planes. In addition, a few very weak diffraction spots or arcs at close vicinity of the {111} and {200} diffraction rings were from the metallic Ti interlayer. After calibration of the image rotation, the direction of the coating growth has been labelled in the SAD pattern. Consequently the imaged area is determined to show a mixed texture.
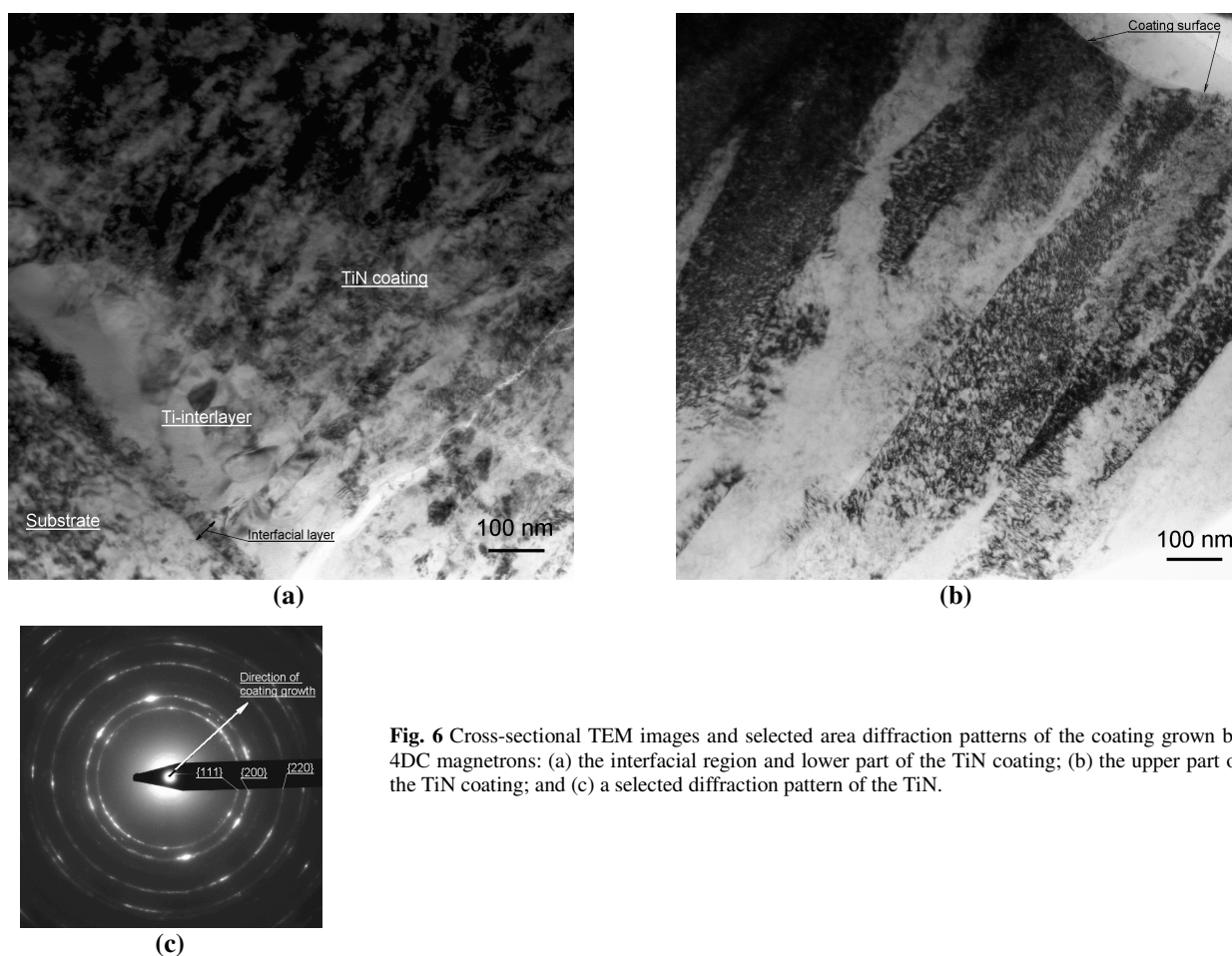

(a)

(b)

(c)

Fig. 6 Cross-sectional TEM images and selected area diffraction patterns of the coating grown by 4DC magnetrons: (a) the interfacial region and lower part of the TiN coating; (b) the upper part of the TiN coating; and (c) a selected diffraction pattern of the TiN.

(a)

(b)

(c)

Fig. 7 Cross-sectional TEM images and selected area diffraction patterns of the coating grown by 3DC+HIPIMS deposition: (a) the interfacial region and lower part of the TiN coating; (b) the upper part of the TiN coating; and (c) a selected diffraction pattern of the TiN.
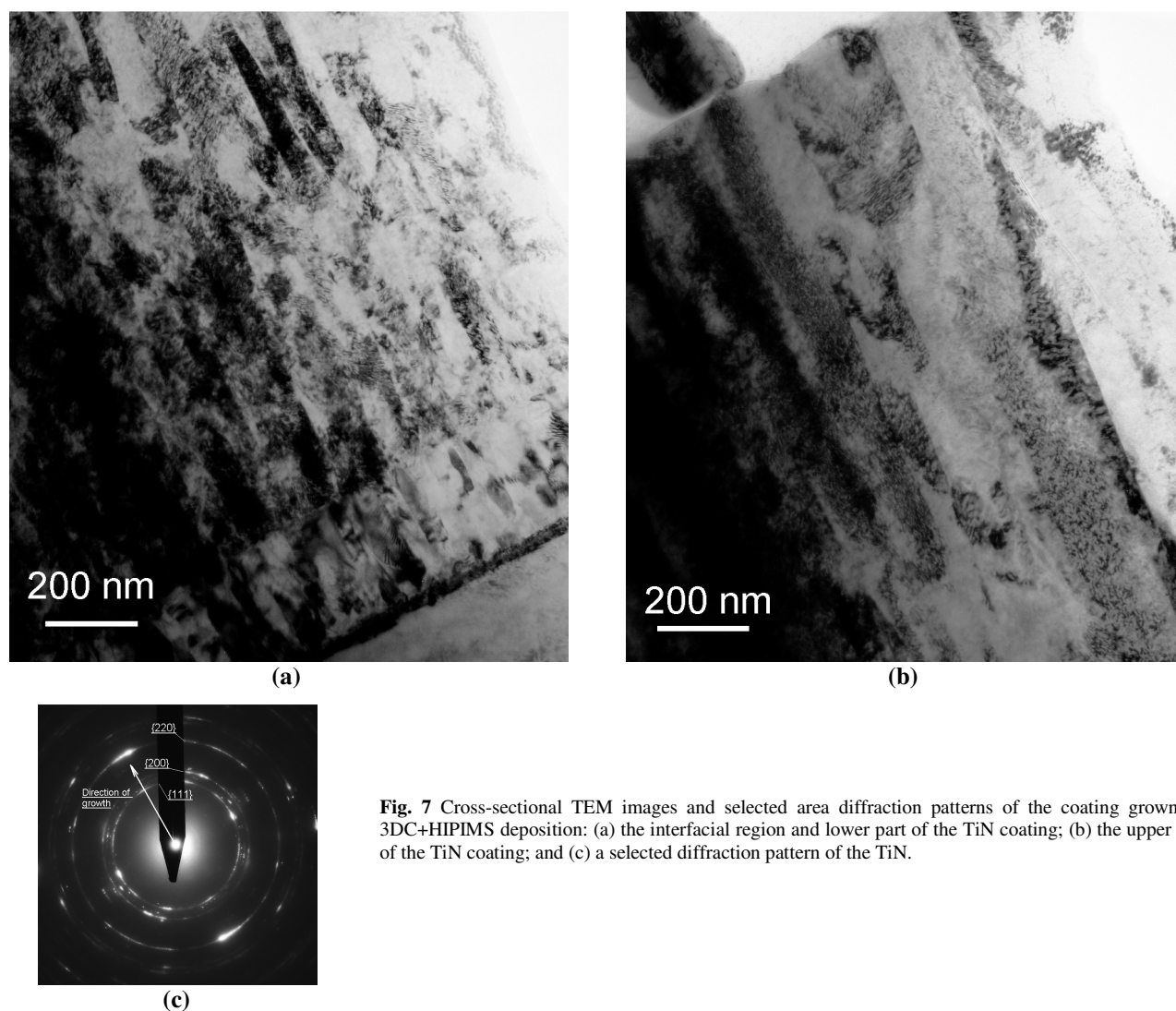
Figure 7 shows XTEM observation and SAD analysis of the 3DC+HIPIMS TiN. Similar to the 4DC magnetron sputtered TiN as shown in Figure 6, the coating shows a layered structure comprising an intermixing layer, a metallic Ti interlayer, and the polycrystalline columnar TiN coating. The entire section of the coating was found to be void-free. The ion-etching induced intermixing layer between the Ti layer and the steel substrate shows sharp dark contrast to the adjacent Ti and substrate. The interface between the TiN and Ti can be easily recognized. The TiN coating has also experienced an evolution from fine columnar grains in the initial growth (Figure 7a) to gradually coarse columns having well-defined boundaries (Figure 7b). However, the lower part of the TiN coating is obviously different from the 4DC magnetron sputtered TiN by showing clearly defined grain boundaries in the nanoscale granular structure, Figure 7a. In Figure 7c, the hybrid TiN coating shows a strong (220) texture as evidenced by the much stronger {220} diffraction than other diffractions at the coating growth direction.

Figure 8 shows Bragg-Brentano XRD curves of the as-deposited samples. Because of the X-ray penetration, each curve contains not only diffraction peaks of the TiN, but also those of the stainless substrate as well as the metallic Ti interlayer. Both coatings show predominantly a single-phase NaCl-type cubic structure and a strong (220) texture. The (220) texture in the 3DC+HIPIMS TiN is even stronger, which can be recognized in the lower intensities of the {111} and {200} diffractions.

In order to investigate the effect of the HIPIMS incorporation on the crystalline structure of the deposited TiN, the obtained XRD data have been quantified in terms of the diffraction peak broadening, the TiN lattice parameter, and residual stress. The results are summarised in Table 1. In the first, both TiN coatings show large broadening of the {111}, {200} and {220} diffractions, whereas the peaks of the 3DC+HIPIMS TiN are slightly and consistently wider than the 4DC magnetron sputtered TiN. The pronounced peak broadening suggests high degree of lattice distortion, and or grain refining, in the as-deposited TiN coatings. Secondly, the 3DC+HIPIMS TiN shows slightly larger lattice parameter than the DC magnetron sputtered TiN. The exact reason for the lattice expansion is not known whereas the significantly higher ionization introduced by the HIPIMS was likely to improve the ionic bonding between the Ti and N atoms or ions. Additionally, the lattice parameters determined from the θ-2θ configuration are higher than the stress-free values (determined in the residual stress calculation). The different values imply a compressive residual stress in both coatings,
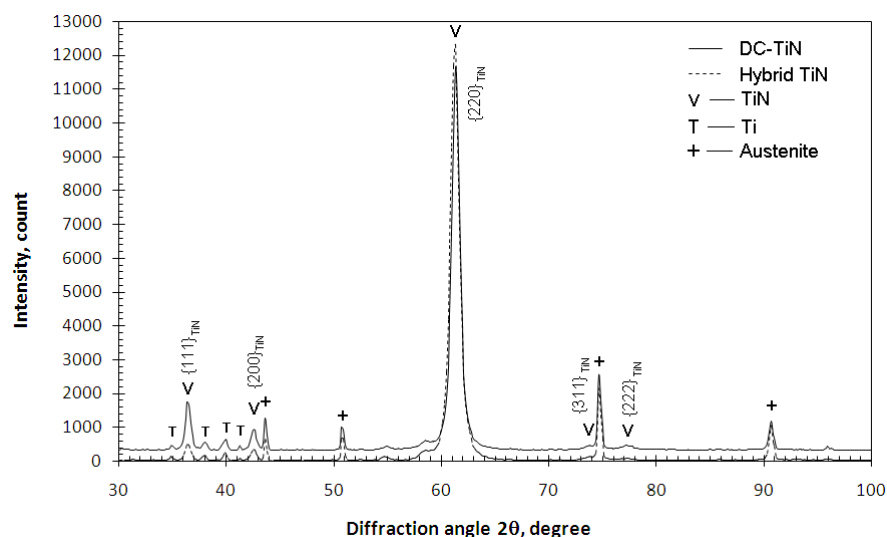
Fig. 8 XRD curves of the TiN coatings acquired at the Bragg-Brentano mode. The sharp peaks labelled '+' are from the stainless steel substrate. The small peaks labelled 'T' are from the Ti interlayer.

Table 1 Crystalline characteristics and residual stress measurements of the TiN coatings.

Properties	4DC - TiN	3DC+1HIPIMS - TiN
Peak broadening (FWHM) degree		
$\beta_{(111)}$	0.561	0.594
$\beta_{(200)}$	0.561	0.594
$\beta_{(220)}$	0.858	0.957
Lattice parameter a_0, nm		
In θ-2θ configuration	0.4262	0.4265
Stress-free value	0.4231	0.4250
Residual stress, GPa		
On (111)	-6.0 ± 0.6	-3.3 ± 0.8
On (220)	-7.9 ± 1.0	-3.2 ± 1.2

being consistent to the stress measurement. Finally, the 3DC+HIPIMS TiN exhibits a compressive residual stress of -3.2 ± 1.2 GPa or -3.3 ± 0.8 GPa, noticeably lower than the 4DC magnetron sputtered TiN.

3.3 Tribological properties

Four sets of unlubricated sliding wear tests have been carried out. Figure 9 shows typical examples of the friction coefficients measured in the wear tests. The measurements of average friction coefficients and wear properties are summarised in Table 2. The depths of the wear tracks created on the coatings ranged from 1.3 to 1.7 µm, well within the coating thickness. Thus the friction and wear properties measured represent properties of the coatings only, i.e. without contribution of the substrate. It has been concluded that, in the employed tribological test conditions, the TiN coating grown by the hybrid 3DC+1HIPIMS deposition has similar tribological properties when compared to the DC magnetron sputtered TiN coating. In Figure 9, both coatings exhibited variation of friction coefficient in the running-in period by starting from a value less than 0.25 and increasing progressively to steady state above 0.9. The average coefficients of friction are 0.84 –
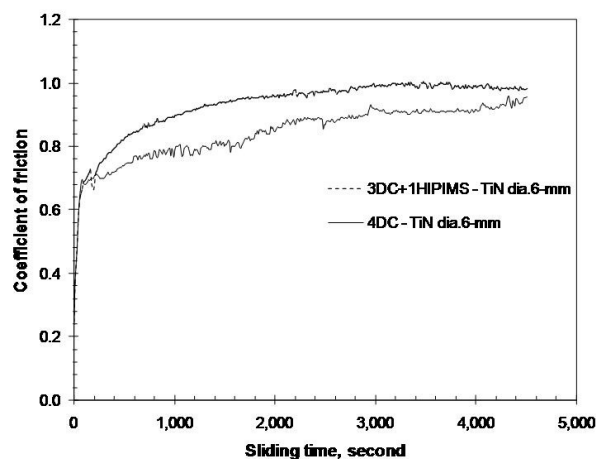

Fig. 9 Typical friction curves of the TiN coatings in un-lubricated sliding against a WC-Co counterpart ball.

0.97, whereas the specific wear coefficients are in the order of 10^{-15} m^{3}N^{-1}m^{-1}.

Table 2 Friction coefficient and wear properties of the TiN coatings.

No.	TiN	Wear track dia.	Sliding time	Coefficient of friction	Coefficient of wear	Wear track depth	Wear track width	Ball wear
		mm	sec.		$\times 10^{-15}$ m^{3}N^{-1}m^{-1}	μm	μm	μm
1	4DC	6	4531	0.84	1.5	1.7	214	228
2	4DC	10	6454	0.97	1.2	1.3	192	221
3	3DC+1HIPIMS	6	4499	0.93	1.2	1.4	207	237
4	3DC+1HIPIMS	10	5404	0.96	2.0	1.6	240	263

Table 3 Analysis of the deposition rates achieved by the 4DC magnetron and the hybrid processes

Properties	4DC - TiN	3DC+1HIPIMS - TiN
The overall deposition rate		
Deposition time, min	44	55
Coating thickness, μm	2.56	2.69
Deposition time, μm/min	0.064	0.049
The layer-by-layer deposition		
Sub-layer period, nm	16	12.2
Grown by each target, nm	4	DC: 3.8
		HIPIMS: 0.9
The layer-by-layer growth of (220)-textured TiN		*($d_{(220)}$ = 0.15 nm)*
Number of (220) layers	107	DC: 75
		HIPIMS: 6

4 Discussion

In this paper, the hybrid HIPIMS and DC magnetron sputtering has demonstrated its advantage in the deposition of TiN coating by showing finer columnar structure, higher hardness and lower residual stress. The overall deposition rate of the hybrid process is approximately 0.049 μm/min, which has been dominated by the DC magnetron components. In particular, the combination of smooth surface, high hardness, strong interfacial adhesion and low residual stress would expect good performance in severe tribological conditions.

4.1 Effect of HIPIMS on deposition rate

Table 3 shows analyses of the TiN deposition rates achieved in the two sputtering processes. The 3DC+1HIPIMS hybrid process showed an overall deposition rate of 0.049 μm/min, whereas the rate of the 4DC magnetron sputtering was 0.064 μm/min. The HIPIMS incorporation led to a decrease in the deposition rate by 0.015 μm/min.

In the four-target configuration as shown in Figure 1, the TiN grew in a layer-by-layer mode when the samples passed the plasma-effective zones in front of every target. As the sample stage was rotating at a constant speed of 4 cycles per minute, the sub-layer period can be determined to be 16 nm, or 4 nm of net deposition from each DC-powered target of the 4DC magnetrons. For the hybrid 3DC+1HIPIMS deposition, the sub-layer period can be estimated to be 12.2 nm. HIPIMS has been known to have dramatically lower deposition rate than DC magnetron

sputtering [2-3, 5-9]. In our practises on sputtering deposition of similar nitride coatings, the deposition rate of a single HIPIMS powered target is approximately 25% of the rate of DC magnetron sputtering for a similar applied power. Applying this ratio to the current case, the contributions have been estimated to be 11.29 nm by the three DC magnetron targets, or 3.76 nm per target, and 0.94 nm by the HIPIMS target respectively. It is noticed that the net contribution of the DC magnetrons in the hybrid configuration, 3.76 nm per target, is slightly lower than that in the 4DC magnetron configuration.

Further analysis can be made if the strong (220) texture of the deposited TiN coatings is considered. Because of the strong (220) texture, most of the columnar grains have their (220) lattice planes parallel to the coating surface. The d-spacings of the (220) planes have been determined to be 0.15 nm. Then in the 4DC magnetron sputtered TiN, each sub-layer of 16 nm in thickness comprises 107 atomic layers along the (220) plane. For the hybrid coating, the numbers of (220) atomic layers deposited by the 3DC magnetrons and by the HIPIMS are 75 and 6 respectively. Obviously the overall deposition rate of the 3DC+1HIPIMS hybrid process was dominated by the three DC magnetrons.

Although the contribution of the HIPIMS to the overall deposition rate was marginal as compared to the three DC magnetrons, however, the species emitted from the HIPIMS-powered target were highly energetic because of the substantially higher ionization than the DC-powered magnetrons. According to the analyses described above, the HIPIMS-emitted species, forming a thin TiN film of six (220)-oriented atomic layers, would have made a bombarding effect on the 75 fresh atomic layers of the DC

magnetron sputtered TiN prior to the HIPIMS deposition. The extra ion bombardment should be the main cause of the subsequent structure evolution.

4.2 Effect of HIPIMS on coating structure

The coating grown by 4DC magnetrons showed a smooth surface, dense columnar structure, strong (220) texture, and excellent adhesion property. According to our knowledge, most of TiN coatings previously reported showed either a (111) texture or a (200) texture [25-26, 30, 32-36]. A (111) texture is usually formed in coatings having high residual stresses in which the formation of (111) texture obeys a mode of minimum strain energy. On the other hand, a (200) texture can be formed either when the controlling factor was the lowest surface energy [37-40] or when highly energetic bombardment was applied to result in re-nucleation during the coating growth [24]. In contrast, (220) texture was rarely found in magnetron sputtered TiN coatings [31], although a few cases were reported in other sputtered coatings of other transition metal nitrides, such as TiAlN/VN [24], TiAlN/CrN [42] and VN [43]. There is still lack of theoretical understanding about the formation of (220) texture. A common feature is that these coatings were grown under insufficient atom mobility provided by relatively low substrate bias voltages less than -80V. A possible explanation for the (220) texture was proposed that, nitrogen atoms in the NaCl-type lattice preferred to form a tetrahedral dumb-bell pair along the [220] direction [44].

The good adhesion property was attributed to the success in the interface strengthening of the combined Ar/Ti ion etching and the metallic Ti interlayer. Such interface strengthening has been applied in various hard coatings in our previous research [20, 45-48]. However, a remarkable structural feature of the DC magnetron sputtered TiN is the high residual stress accompanying the competitive columnar growth, as shown in Table 1. The formation of high residual stress is consistent to the author's previous study in magnetron sputtered TiAlN/VN nitride coatings that high residual compressive stresses were measured when the applied substrate bias voltage was higher than -85V [25]. More research on the structure formation of magnetron sputtered coatings can be found in literature [25, 49-50].

The coating grown by 3DC+1HIPIMS remained the same surface morphology and strong (220) texture as the 4DC-magnetron sputtered coating, because the coating growth, along with the deposition rate, was dominated by the 3DC magnetrons. Despite these, the HIPIMS has shown remarkable influence on the structure of the deposited coating, including columnar grain refining, stronger texture and lower residual stress. It was reported that ion flux provided by a highly pulsed magnetron made more effective conversion of energy in thin film deposition [49]. TiN coatings grown purely by HIPIMS deposition showed refined columnar grains due to the formation of re-nucleation islands as a result of the increased adatom mobility [31-32]. In the four-target deposition in multilayer mode, the flux of Ti ions emitted from the HIPIMS-powered target would bring about additional adatom mobility to the 75 fresh atomic layers of (220)-textured TiN deposited by the three DC targets, which consequently

resulted in dynamic recovery of point defects in the highly distorted lattice, such as reducing the number of entrapped nitrogen and argon atoms and filling-up atomic-scale voids. Such multilayer growth model in hybrid HIPIMS and unbalanced magnetron deposition has recently been suggested in Ref [18], although the multilayer structure was not traceable in XTEM observation. Because of the partial recovery of point defects in the magnetron sputtered TiN lattice, the column grains were observed to show well defined boundaries in the XTEM observation. The residual stress was substantially lower than the DC magnetron sputtered TiN. The lower residual stress agrees well to the results of other researchers [16-19]. In addition, it should be pointed out that, the hardness values measured by indentation are related to the residual stress of the coatings. It is know that compressive residual stress can restrict the deformation depth and thereafter gives rise to higher hardness value. In the current experiments, the 4DC magnetron sputtered TiN showed a hardness value of 34.8 GPa given a compressive residual stress of -7.9 GPa (the value determined using the {220} plane, Table 1). Having lower residual stress of -3.2 GPa, the hybrid TiN coating showed even higher hardness than the DC magnetron sputtered TiN. The higher hardness should be attributed to the finer columnar grain size and high density of lattice distortion as well as improved coating density. It is suggested to perform more precise analysis, such as high resolution electron microscopy, to find more details of lattice structural changes. Nevertheless, a decrease of the residual compressive stress, while maintaining the high hardness, would be an advantage for high resistance to severe wear. In conventional magnetron sputtering, a negative substrate bias voltage is usually applied to improve the structure densification of the deposited coatings, which however inevitably results in high residual compressive stresses in the coatings, e.g. as being measured in this study and shown in literature [24, 42, 51-53]. Such residual stresses are known to be deteriorating to the adhesion property of hard coatings, especially for those to be used under severe tribological loading conditions. In such circumstances, the incorporation of a HIPIMS component in a multi-target magnetron process, as being demonstrated in the current research, would be expected to be beneficial to the overall mechanical properties and tribological performance.

4.3 About the friction and wear of the TiN coatings

In the current experiments, the two TiN coatings showed similar friction and wear properties under the applied test conditions. The results suggest that, the tribological properties were determined predominantly by the intrinsic properties of the TiN nitride itself whereas the incorporation of HIPIMS in the deposition had marginal influence. The friction coefficient and wear properties measured in current experiments are in good agreement to previous research [54-56]. In each sliding wear test, the gradual increase of friction from a low value to a relatively steady value obeys the general rule of the running-in friction of most transition metal nitride coatings in unlubricated sliding wear [57-58]. In Ref. [57], it has been revealed that, the running-in process is associated with

initial abrasive wear of the TiN coatings under the asperity contacts with the counterpart surfaces, leading to the generation of wear particles. The origin of friction in the running-in period comprises the resistant forces arising from the generation of wear particles and the subsequent complex interactions between the wear particles within the sliding contact zone, namely their sliding and rolling motions, plastic deformation of the worn surfaces, the breaking/powdering of the wear debris and the simultaneous thermal and chemical interactions, as well as the interactions with the environment species and so on. The complex interactions eventually lead to the formation of a well-adhered tribofilm on the top of the worn surfaces. After that, the steady friction coefficient is dominated by the shear deformation of the tribofilm, and the wear rate by the tribo-chemical reaction between the tribofilm and the nitride surface as well as the nano-scale delamination wear [58]. In such circumstances, the coating hardness is not a controlling factor to the friction and wear.

5 Conclusions

A hybrid magnetron sputtering process has been developed in a closed field unbalanced magnetron sputtering (CFUBMS) configuration, comprising three DC magnetrons and one magnetron with a HIPIMS power supply. A TiN coating grown by using the hybrid magnetron sputtering process has been experimentally compared with another TiN coating grown purely by DC magnetron sputtering. The following conclusions can be made from the experiment results.

(1) The hybrid process achieved a deposition rate of 0.049 μm /min, which was dominated by the three DC magnetron targets, whereas the HIPIMS incorporation showed marginal contribution.

(2) The HIPIMS incorporation has led to significant decrease in the residual compressive stress from -6.0 to -3.5 GPa, and an increase of the coating hardness from 34.8 to 38.0 GPa. Both the hybrid and DC magnetron sputtered coatings exhibited dense columnar structure, smooth coating surfaces, and NaCl-type cubic crystalline structure with a strong (220) texture.

(3) A 30-50 nm thick interfacial ion-mixing layer has been observed on the ion-etched substrate surface, which combined with the metallic Ti base layer contributed to excellent adhesion property.

(4) The TiN coatings showed friction coefficients in a range of 0.8 - 0.9 and a wear coefficient of the order of $10^{-15}\,m^3N^{-1}m^{-1}$, regardless of the deposition techniques.

References

[1] V. Kouznetsov, K. Macak, J. Schneider, U. Helmersson, I. Petrov, Surf. Coat. Technol. 122 (1999) 290.

[2] B. Vyse, J. M. Gissing, Spectra of short, locked magnetron pulses, IEEE Transactions on Electron Devices Ed18, 1971, 221.

[3] I. M. Vigdorchik, V. D. Naumenko, V. P. Timofeev, Dopovidi Akademii Nauk Ukrainskoi RSR Seriya A-Fiziko-Matecatichni Ta Technichni Nauki 7 (1975) 633.

[4] R. K. Parker, W.M. Black, R. Tobin, M. Herndon, V.L. Granatstein, G. Farney, Bulletin of the American Physical Society 23 (1978) 863.

[5] P. M. Tyuryukanov, I. K. Fetisov, A. D. Nikolskii, Zhurnal Tekhnicheskoi Fiziki 51 (1981) 2018.

[6] R. Gruen, Process and apparatus for coating conducting pieces using a pulsed glow discharge, US Patent 5015493, May 14, 1991.

[7] D. V. Mozgrin, I. K. Fetisov, G.V. Khodachenko, Plasma Phys. Rep. 21 (1995) 401.

[8] S. P. Bugaev, N. N. Koval, N. S. Sochugov, A. N. Zakharov, Investigation of a high-current pulsed magnetron discharge initiated in the low-pressre diffuse arc plasma, XVIIth International on Discharges and Electrical Insulation in Vacuum, 1996, p. 1074.

[9] I. K. Fetisov, A. A. Filippov, G. V. Khodachenko, D. V. Mozgrin, A. A. Pisarev, Vacuum 53 (1999) 133.

[10] U. Helmersson, M. Lattemann, J. Bohlmark, A. P. Ehiasarian, J. T. Gudmundsson, Thin Solid Films 513 (2006) 1.

[11] K. Sarakinos, J. Alami, S. Konstantinidis, Surf. Coat. Technol. 204 (2010) 1661.

[12] J. Alami, P. Eklund, J. Emmerlich, O. Wilhelmsson, U. Jansson, H. Högberg, L. Hultman, U. Helmersson, Thin Solid Films 515 (2006) 1731.

[13] J. Alamia, K. Sarakinos, G. Mark, M. Wuttig, Appl. Phys. Lett. 89 (2006) 154104.

[14] G. West, P. Kelly, P. Barker, A. Mishra, J. Bradley, Plasma Process. Polym. 6 (2009) S543.

[15] D. Lundin, C. Huo, N. Brenning, M. A. Raadu, U. Helmersson, Deposition Rate Loss in High Power Impulse Magnetron Sputtering: Understanding through computational modelling, 54th Annual Technical Conference Proceedings, Chicago, IL April 16–21, 2011, 172.

[16] J. Lin, W. D. Sproul, J. J. Moore, Z. Wu, S. Lee, R. Chistyakov, B. Abraham, JOM 63 (2011) 49.

[17] J. Lin, W.D. Sproul, J. J. Moore, S. Lee, S. Myers, Surf. Coat. Technol. 205 (2011) 3226.

[18] J. Paulitsch, M. Schenkel, Th. Zufra, P.H. Mayrhofer, W.-D. Münz, Thin Solid Films 518 (2010) 5558.

[19] G. Greczynski, J. Lua, M. Johansson, J. Jensen, I. Petrov, J. E. Greene, L. Hultman, Vacuum 86 (2012) 1036.

[20] S. Yang, X. Li, K. E. Cooke, D. G. Teer, Appl. Surf. Sci. 258 (2012) 2062.

[21] J. Lin, J. J. Moore, W. D. Sproul, S. L. Lee, J. Vac. Sci. Technol. 29A (2011) 061301.

[22] M. Audronis, V. Bellido-Gonzalez, R. Brown, Thin Solid Films 520 (2011) 1571.

[23] Q. Luo, A. H. Jones, Surf. Coat. Technol. 205 (2010) 1403.

[24] Q. Luo, D. B. Lewis, P. Eh. Hovsepian, W. –D. Münz, J. Mater. Res. 19 (2004) 1093.

[25] L. Hultman, W-D. Münz, J. Musil, S. Kadlec, I. Petrov, and J. E. Greene, J. Vac. Sci. Technol. A9 (1991) 434.

[26] I. Petrov, F. Adibi, J. E. Greene, L. Hultman, and J. -E. Sundgren, Appl. Phys. Lett. 63 (1993) 36.

[27] K. P. Shaha, Y. T. Pei, C. Q. Chen, A. A. Turkin, D. I. Vainshtein, J. Th. M. De Hosson, Appl. Phys. Lett. 95 (2009) 223102.

[28] C. Schonjahn, M. Bamford, L. A. Donohue, D. B. Lewis, S. Forder, W.D. Münz, Surf. Coat. Technol. 125 (2000) 66.

[29] C. Schonjahn, L. A. Donohue, D. B. Lewis, W. D. Münz, R. D. Twesten, I. Petrov, J. Vac. Sci. Technol. A18 (2000) 1718.

[30] J. Paulitsch, P. H. Mayrhofer, W. -D. Münz, M. Schenkel, Thin Solid Films 517 (2008) 1239.

[31] M. Lattemann, A. P. Ehiasarian, J. Bohlmark, P. Å. O. Persson, U. Helmersson, Surf. Coat. Technol. 200 (2006) 6495.

[32] F. Magnus, A. S. Ingason, O. B. Sveinsson, S. Olafsson, J. T. Gudmundsson, Thin Solid Films 520 (2011) 1621.

[33] J. S. Chun, I. Petrov, J. E. Greene, J. Appl. Phys. 86 (1999) 3633.

[34] J. E. Greene, J. E. Sundgren, L. Hultman, I. Petrov, D. B. Bergstrom, Appl. Phys. Lett. 67 (1995) 2928.

[35] T. Q. Li, S. Noda, Y. Tshji, T. Ohsawa, H. Komiyama, J. Vac. Sci. Technol. A20 (2002) 583.

[36] R. Banerjjee, K. Singh, P. Ayyub, M.K. Totlani, A.K. Suri, J. Vac. Sci. Technol. A21 (2003) 310.

[37] G. Knuyt, C. Quaeyhaegens, J.D. Haen, and L. M. Stals, Surf. Coat. Technol. 76 (1995) 311.

[38] G. Knuyt, C. Quaeyhaegens, J. D Haen, and L. M. Stals, Thin Solid Films 258 (1995) 159.

[39] U. C. Oh, J. H. Je, J. Appl. Phys. 74 (1993) 1692.

[40] C. M. Cotell, J. K. Hirvonen, Surf. Coat. Technol. 81 (1996) 118.

[41] M.I. Jones, I.R. McColl, D. M. Grant, Surf. Coat. Technol. 132 (2000) 143.

[42] W. -D. Münz, D. B. Lewis, P. Eh. Hovsepian, C. Schönjahn, A. Ehiasarian, I. J. Smith, Surf. Eng. 17 (2001) 15.

[43] G. Farges, E. Beauprez, and M. C. Staine Catherine, Surf. Coat. Technol. 61 (1993) 238.

[44] A. J. Perry, V. Valvoda, D. Rafaja, Vacuum 45 (1994) 11.

[45] S. C. Yang, E. Eiemann, D. G. Teer, Surf. Coat. Technol. 188 (2004) 662.

[46] S. Yang, K. E. Cooke, X. Li, F. McIntosh, D. G. Teer, J. Phys D – Appl. Phys. 42 (2009) 104001.

[47] Y. J. Shi, S. Y. Long, S. C. Yang, F. S. Pan, Vacuum 84 (2010) 962.

[48] S. C. Yang, K. Cooke, A. Aramcharoen, P. Mativenga, D. Teer, Mater. Technol. 26 (2011) 20.

[49] Y. T. Pei, C. Q. Chen, K. P. Shaha, J. Th. M. De Hosson, J. W. Bradley, S. A. Voronin, M. Cada, Acta Mater. 56 (2008) 696.

[50] K. P. Shaha, Y. T. Pei, C. Q. Chen, A. A. Turkin, D. I. Vainshtein, App. Phys. Lett. 95 (2009) 223102.

[51] H. Oettel, R. Wiedemann, Surf. Coat. Technol. 76-77 (1995) 265.

[52] S. Imamura, H. Fukui, A. Shibata, N. Omiri, M. Setoyama, Surf. Coat. Technol. 202 (2007) 820.

[53] L. Zhou, C. Y. Wang, Z. Qin, Proceedings of The Institute of Mechanical Engineers Part B: Journal of Engineering Manufacture 223 (2009) 267.

[54] E. Vancoille, B. Blanpain, X. Ye, J. P. Celis, J. R. Roos, J. Mater. Res. 9 (1994) 992.

[55] M. Z. Huq, J. P. Celis, Wear 212 (1997) 151.

[56] E. Badisch, G.A. Fontalvo, M. Stoiber, C. Mitterer, Surf. Coat. Technol. 163–164 (2003) 585.

[57] Q. Luo, Tribo. Lett. 37 (2010) 529.

[58] Q. Luo, Z. Zhou, W. M. Rainforth, M. Bolton, Tribo. Lett. 34 (2009) 113.